Paper:

Extraction of Collapsed Bridges Due to the 2011 Tohoku-Oki Earthquake from Post-Event SAR Images

Wen Liu[†] and Fumio Yamazaki

Graduate School of Engineering, Chiba University
1-33 Yayoi-cho, Inageku, Chiba 263-8522, Japan
[†]Corresponding author, E-mail: wen.liu@chiba-u.jp

Since synthetic aperture radar (SAR) sensors onboard satellites can work under all weather and sunlight conditions, they are suitable for information gathering in emergency response after disasters occur. This study attempted to extract collapsed bridges in Iwate Prefecture, Japan, which was affected by more than 15-m high tsunamis due to the Mw 9.0 earthquake on March 11, 2011. First, the locations of the bridges were extracted using GIS data of roads and rivers. Then, we attempted to detect the collapsed or washed-away bridges using visual interpretation and thresholding methods. The threshold values on the SAR backscattering coefficients and the percentage of non-water regions were applied to the post-event high-resolution TerraSAR-X images. The results were compared with the optical images and damage investigation reports. The effective use of a single SAR intensity image in the extraction of collapsed bridges was demonstrated with a high overall accuracy of more than 90%.

1. Introduction

Road networks are often fragmented after an earthquake due to strong shaking or secondary effects, e.g., tsunami, landslide, and liquefaction. However, road networks are essential components of the emergency response. In the March 11, 2011 Tohoku-oki, Japan, earthquake and associated tsunamis, many bridges in Iwate and Miyagi Prefectures were washed away by tsunamis [1, 2]. In addition, debris carried by tsunamis and the inundation caused road closures in a wide area remained over a long period of time. Owing to the increased risk for emergency responders and the wide range of affected areas, it is often difficult to grasp the extent of the damage by field surveys. Under these situation, remote sensing is an effective tool for emergency response.

Optical images have been used for damage assessment in recent decades [3–5]. Although optical images can provide easy-to-understand information, they are affected by weather conditions. Thus, synthetic aperture radar (SAR), which is essentially not affected by weather and sunlight conditions, is more effective in emergency response. Owing to remarkable improvements in SAR sensors, high-resolution TerraSAR-X (TSX) and COSMO-SkyMed (CSM) SAR images are available with ground resolution of 1 to 5 m, and the observation of manmade structures in urban areas is now possible. Various damage detection methods using multi-temporal SAR images taken before and after a disaster have been proposed [6–8]. Damage assessments for a single building have also been carried out in previous studies [9–12]. However, a pre-event SAR image taken by the same acquisition condition is not available in many cases. Owing to the side-looking nature of SAR, layover of buildings and multi-bounce of radar occur between the ground and buildings. The backscattering model of an individual building is useful to estimate the building height information [13] and damage situation [14] from a single SAR intensity image.

As an important part of road networks, bridges were also recognized in remote sensing images [15–19]. Damage assessments of bridge structures due to the 2011 Tohoku-oki earthquake have been conducted in several researches. Akiyama et al. [20] estimated bridge failure probability using the tsunami hazard and fragility curves. Shoji and Nakamura [21] assessed the tsunami damage to girder-type road bridges considering the inundation depth, the ratio of the inundation depth to the girder elevation, and the flow velocity. In our previous study [22], we detected the bridges damaged in Miyagi Prefecture using the pre- and post-event TSX images. However, studies on damage detection of bridges due to earthquakes or tsunamis from SAR imagery are limited. Jiang et al. [23] demonstrated the possibility of observing bridge damage from L-band airborne SAR images. Balz et al. [24] attempted to identify damaged/collapsed bridges using TSX and CSM images and found limitations in the identification of damaged bridges using only one SAR image; however, the study considered only a small number of bridges. In addition, only visual interpretation was carried out from a post-event SAR image. Thus, an automated method to extract damaged bridges in a wide area from a single post-event SAR image is necessary.

In this paper, we investigated the detection of collapsed or washed-away bridges due to the 2011 Tohoku-oki earthquake by setting a proper threshold value using post-event TSX intensity images and GIS data. To ver-
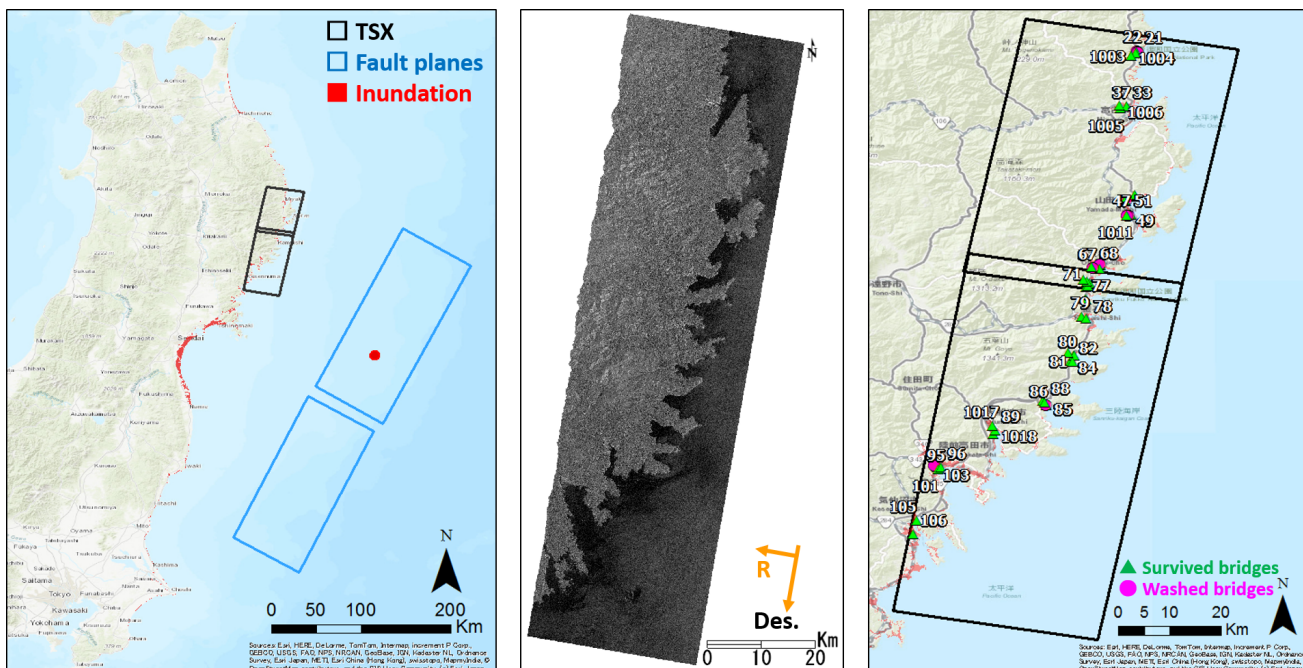
Fig. 1. (a) Study area covers Iwate Prefecture, Japan; (b) post-event mosaiced TSX image after the pre-processing steps; (c) locations of the 58 target bridges, where Nos. 21 to 105 are the bridges reported by the NILIM [1] and Nos. 1001 to 1018 are not in the reports.

ify the accuracy, the obtained results were compared with optical images and field investigation reports.

2. Study Area and Imagery Data

The study area was set in the Pacific coast of the Tohoku region, Japan, which was damaged severely by the 2011 Tohoku-oki earthquake and the resultant tsunamis, as shown in **Fig. 1(a)**. In Iwate Prefecture, the inundation reached a total area of 58 km² and more than 18 thousand buildings were collapsed or washed away due to the huge tsunamis. The reported flooded regions are also shown in **Fig. 1(a)** by red color [25].

Two TSX intensity images taken on March 12, 2011 (20:43 UTC), 1.5 days after the tsunami, were used in this study. The images were acquired in the StripMap mode by HH polarization. The spatial resolutions were 3.05 m in the azimuth direction and 3.01 m in the range direction. The incident angle at the center of the images was approximately 33.2°, and the heading angle was approximately 190.4° in the descending path with the right-look. They were provided as EEC (enhanced ellipsoid corrected) products, which were already orthorectified and multi-look compressed by the satellite owner (The German Aerospace Center: DLR). These products were projected to the World Geodetic System (WGS) 84 reference ellipsoid with a resampled square pixel-size of 1.25 m. In addition, the image distortion caused by the terrain height has been compensated for by a globally available digital elevation model (SRTM: the Shuttle Radar Topography Mission).

Radiometric calibration and speckle filter were applied

as pre-processing. Two SAR intensity images were transformed from a 16-bit digital number (DN) to a backscattering coefficient (sigma naught) in the dB unit according to the calibration factor [26]. The influence of the incidence angle was also removed in this radiometric calibration. Then, the enhanced Lee filter [27] was applied to reduce speckle noise. Considering the balance between the loss of detailed information and the reduction of speckle noise, a 5×5 pixels window size was adopted in this study. The pre-processed TSX images were mosaicked as one post-event intensity image as shown in **Fig. 1(b)**.

3. Extraction of Target Bridges

Since GIS data of the bridges is not available, the shapes of the bridges were created using data from roads and rivers. A GIS dataset, including water and road boundary lines, was downloaded from the Fundamental Geospatial Data [28]. The roads over water polygons were considered as bridges and were extracted by polygons. Thus, the embankment parts on both ends of the decks were not included. An example of the bridge extraction is shown in **Fig. 2**. Considering the spatial resolution of the TSX images, only the created polygons longer than 10 m in length and larger than 60 m² in size were extracted as the targets. Since the GIS dataset provided by the Geospatial Information Authority of Japan (GSI) was updated in 2016, several washed-away bridges were removed from the dataset. The polygons of these bridges were created manually according to an old map. Finally, 58 bridges were extracted in the study area.

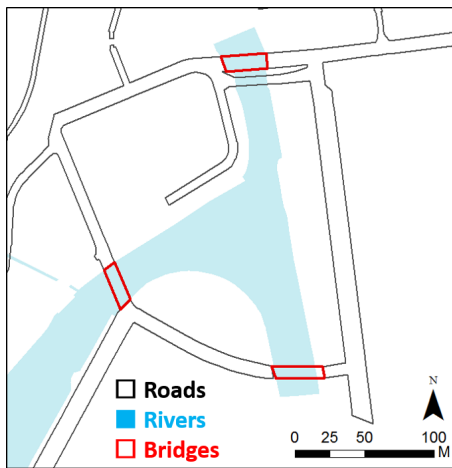The National Institute for Land and Infrastructure Man-

Fig. 2. Example of bridge extraction according to GIS data of roads and water downloaded from the Fundamental Geospatial Data of the GSI [28].

Table 1. Detailed information for the 40 target bridges in the study area investigated by the NILIM [1].

No.	Length [m]	Width [m]	Clearance [m]	Structural type	Washed-away part
21	36.20	9.24	0.80	PC-T girder	superstructure
22	31.40	10.20	2.98	PC-T girder	superstructure
33	103.97	9.40	4.28	Steel box girder	
37	195.60	6.00	3.95	RC-T girder	
43	80.00	8.20	3.50	PC box girder	
45	54.00	2.10	2.15	Steel H girder	super- and sub-structure
46	24.60	4.03	2.02	RC-T girder	
47	60.00	8.30	7.60	PC box girder	
49	16.80	5.60	1.20	PC-T girder	superstructure
51	44.10	6.60	1.10	Steel H girder	superstructure
59	85.60	11.30	3.70	PC-T girder	
61	76.00	5.50	3.34	PC-T girder	super- and sub-structure
62	85.00	3.45	5.39	PC floor slab	
64	63.00	12.50	6.78	Steel I girder	
66	86.50	12.80	5.90	PC floor slab	
67	63.40	9.40	5.74	Steel H girder	
68	66.80	2.70	5.72	PC-T girder	super- and sub-structure
70	145.95	5.80	5.20	Steel H girder	
71	79.20	12.80	6.50	PC-T girder	
73	29.00	12.80	4.30	PC floor slab	
74	34.00	5.84	5.50	Steel I girder	
76	30.00	9.20	10.24	Steel I girder	
77	28.64	8.20	3.70	Steel I girder	
78	108.60	14.32	3.14	Steel I girder	
79	108.00	20.00	3.40	Steel I girder	
80	43.30	9.50	4.95	PC floor slab	
81	68.00	8.40	4.95	Steel I girder	
82	38.40	5.20	4.33	PC box girder	
83	34.00	5.17	7.11	RC-T girder	
84	40.00	9.20	15.80	PC-T girder	
85	9.40	5.80	5.32	PC-T girder	superstructure
86	19.90	5.80	5.32	PC-T girder	
88	14.50	7.80	8.00	RC floor slab	
89	156.90	12.00	2.24	Steel I girder	
95	4.70	8.20	1.60	PC floor slab	
96	56.00	12.80	1.95	PC floor slab	
101	108.74	13.30	6.33	Steel T girder	superstructure
103	147.20	8.20	3.57	Steel truss	superstructure
105	45.00	10.30	1.03	Steel H girder	
106	88.30	16.00	1.87	Steel I girder	

Note: PC denotes prestressed concrete, and RC denotes reinforced concrete.

agement (NILIM) investigated the damage situations of 200 bridges in Iwate, Miyagi, and Fukushima Prefectures by field surveys [1]. Among the investigated bridges, 40 bridges were extracted as the targets using GIS data. Details and damage conditions of the extracted bridges are summarized in **Table 1**. The decks of 10 bridges were reported as washed away, and the substructure of 3 out of these 10 bridges were also washed away. Since the TSX images used in this study have a spatial resolution of approximately 3 m, it is difficult to extract smaller damage levels than collapsed or washed-away. The use of airborne SAR should be considered to extract smaller damage levels.

The 40 investigated bridges were labeled using the same numbers used in the NILIM report from 21 to 106. The 18 bridges without field surveys were labeled in an ascending order from the north to the south, starting from 1001 to 1018. The locations of all the target bridges are shown in **Fig. 1(c)**.

4. Backscattering Model

Bridges over water show complex backscattering patterns including layovers, double-bounce, and triple refection, which are different from buildings [16]. When a bridge has a high elevation from water, three parallel lines can be observed in very high-resolution SAR images. However, for small bridges with insufficient heights, three backscatter signals are overlapped [29]. In this study, most of the target bridges matched the latter case. The backscattering model for small bridges is shown in **Fig. 3**. The simulated backscattering patterns are also shown in the bottom part of **Fig. 3**. The backscattering intensity from each part is manually drawn using the following rule:

double-bounce from the side > reflection from the side > reflection from the top of the deck > triple reflection from the bottom of the deck.

According to the simulated backscattering pattern, a high backscattering coefficient would show in the layover range. Thus, the created bridge polygons should be moved to the sensor direction to cover the layovers. The distance (L) between the layover and the original location depends on the incident angle and the height of the bridge. For the 40 investigated bridges, the clearance heights between the deck and water were reported as presented in **Table 1**. For the other 18 bridges, the heights are unknown. A histogram of the known clearances is shown in **Fig. 4**. The heights of 80% of the bridges are mostly between 2 m to 6 m. Thus, 6 m was adopted as the representative height for the shifting. Based on the 33.2° incident angle and the 280.4° range direction, the bridge polygons moved 9.02 m to the east and 1.66 m to the south. To verify the movement, a comparison of the backscattering coefficients within the original polygons and the moved
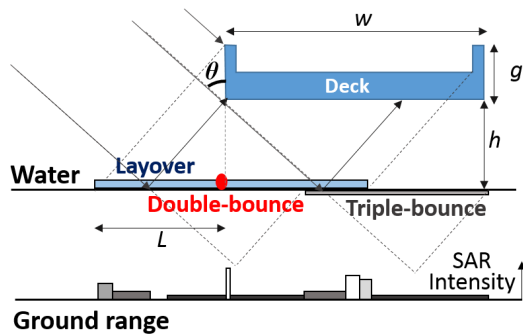
Fig. 3. Backscattering model of small-scale bridges over water.
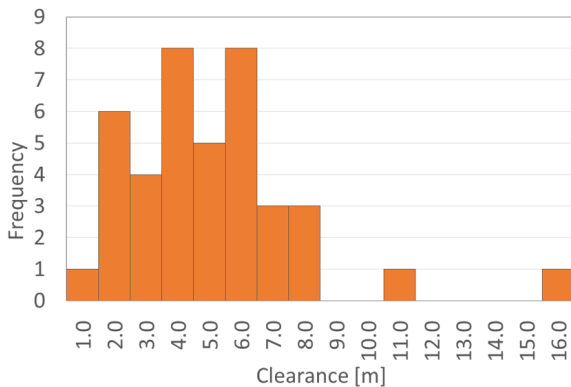

Fig. 4. Histogram of the clearance heights for the 40 bridges investigated by the NILIM.

polygons was carried out. More than half of the bridges showed an increased backscattering intensity within the new polygons, which indicates that the shift made the polygons fit the strong reflected regions better.

The illumination angle between the range and the bridge-axial direction, as well as types of bridges are confirmed as important elements for the appearance of the bridges in SAR images [30]. According to **Table 1**, most of the target bridges were girder or floor slab types of a simple structure. Only No.103 was a steel truss bridge, which was reported as washed-away. Thus, the influence of types of structure could be ignored. The effects of illumination angles were also ignored for the 3-m resolution of the SAR image.

5. Damage Detection of Bridges

5.1. Visual Interpretation

Visual interpretation was first carried out using the polygons of bridges and post-event TSX intensity image. The existence of consecutively high backscatter coefficient within the polygons was the criterion for the interpretation. Eleven bridges were classified as washed-away whereas 47 bridges survived. Then, the result was compared with the report by the NILIM. The error matrix is presented in **Table 2**. A comparison of the NILIM's field survey report and optical images shows that 2 sur-

Table 2. Error matrix for visual interpretation using the shifted polygons of bridges and the post-event TSX intensity image.

		Report of the NILIM			
		Washed-away	Survived	Total	User Acc.
TerrSAR-X	Washed-away	9	2	11	82%
	Survived	1	46	47	98%
	Total	10	48	58	
	Producer Acc.	90%	96%		**95%**

vived bridges were misclassified as washed-away and one washed-away bridge could not be identified. The overall accuracy was 95%, and the Kappa coefficient was 0.83, showing very good agreement with the reference data.

The parts of the TSX image around the 10 washed-away bridges and the 2 misclassified bridges were extracted and shown in **Figs. 5–7**. The pre- and post-event optical images were obtained from Google earth and are also shown in the figures to support the understanding of the SAR image. In the figures, the solid frames show the original locations of bridges and the dashed frames show the shifted shapes. The washed-away bridges were enclosed by red lines and the survived bridges by green lines. Other than bridge No.85, the entire decks of the 9 damaged bridges were completely washed away.

Bridge No.22, which is shown in **Fig. 5**, was the omitted bridge in the visual interpretation. Strong reflection from the survived pier is observed in the middle of the river. Apart from the pier, other parts with high backscattering are seen within the bridge polygon, which is speculated as the reflection from the accumulated debris carried by the tsunamis. Owing to these parts with high backscattering coefficients, this bridge was misclassified as survived.

Bridge Nos.66 and 76, shown in **Fig. 7**, were the survived bridges that were judged as washed-away. Bridge No.66 is behind a water gate in the range direction. It is located in the radar shadow region of the water gate, which resulted in low backscattering intensity in the TSX image. Thus, we misclassified it as washed-away. Bridge No.76 is part of the national highway No.45 with a 10-m clearance height. Although the bridge polygon has been shifted to the sensor direction, it still did not cover the layover region of this bridge. The misclassification was due to the low backscattering intensity in the radar shadow area.

5.2. Thresholding Methods

Although visual interpretation had high accuracy in the damage detection of bridges, high costs in terms of human resources and time are required. Thus, an automated method using image analysis is useful for detecting bridge damages in a wide range. The thresholding method is one of the most common tools for target detections. To estimate a proper threshold value, the statistics of the target bridges were calculated. The average values of the
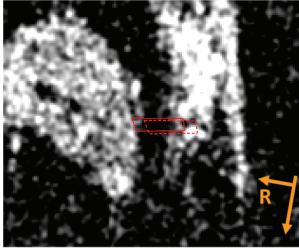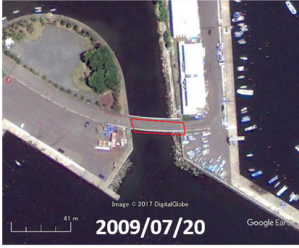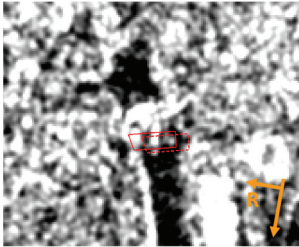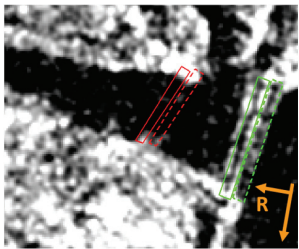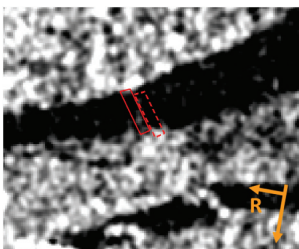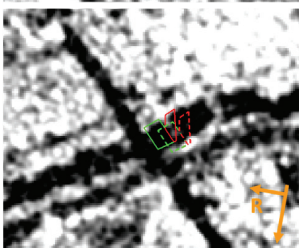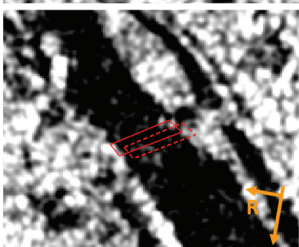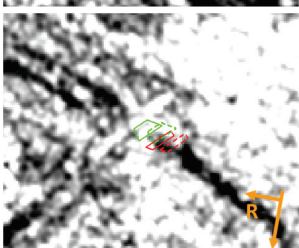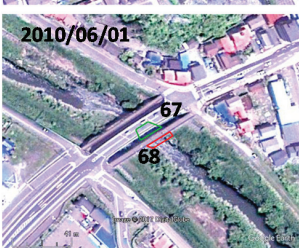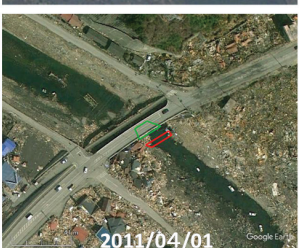
Bridge No.	Post-event TSX	Pre-event optical image	Post-event optical image

Fig. 5. Enlarged images for the washed-away bridges from Nos.21 to 68, where the solid frames are the original polygons and the dashed frames are the shifted ones. The washed-away bridges are shown in red color whereas the survived ones in green color.

Bridge No.	Post-event TSX	Pre-event optical image	Post-event optical image
85		85 86 2010/05/18	2011/04/01
101		2010/07/23	2011/04/01
103		2010/07/23	2011/03/13
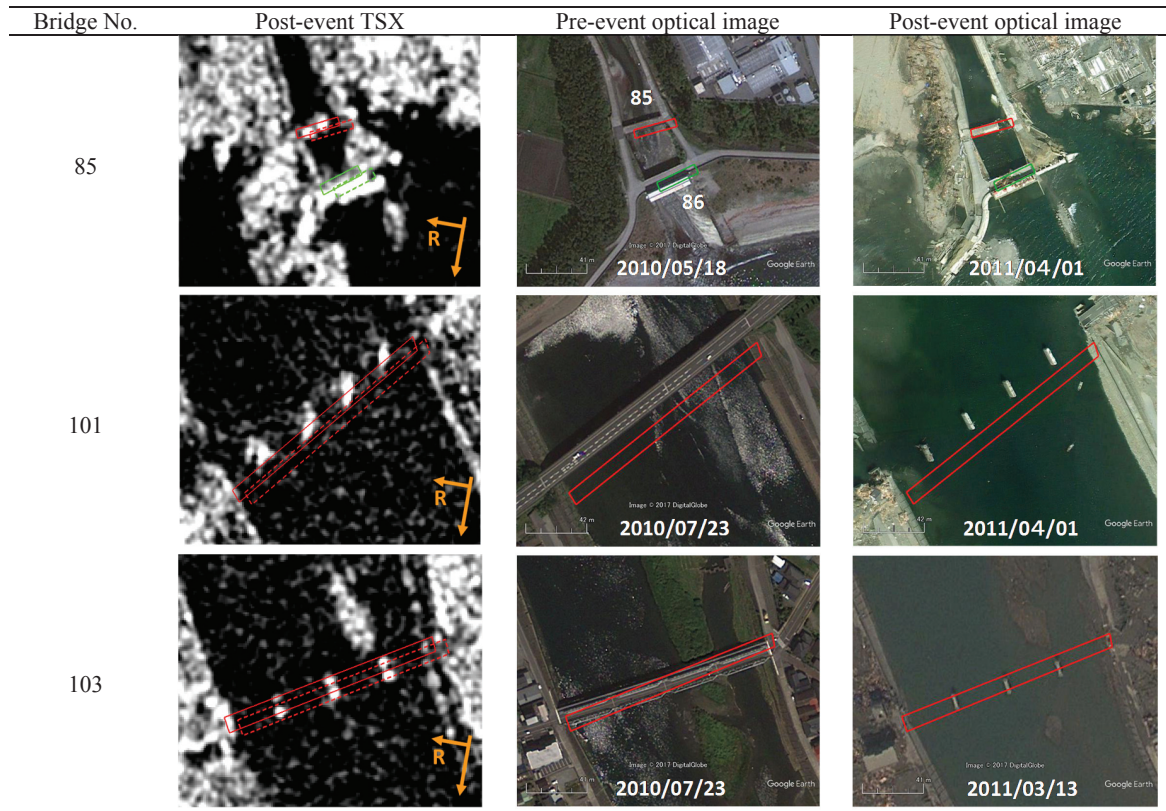
Fig. 6. Enlarged images for the washed-away bridge Nos.85, 101, and 103.

Bridge No.	Post-event TSX	Pre-event optical image	Post-event optical image
66		2010/06/01	2011/03/24
76		2010/06/01 77 76	2011/04/01
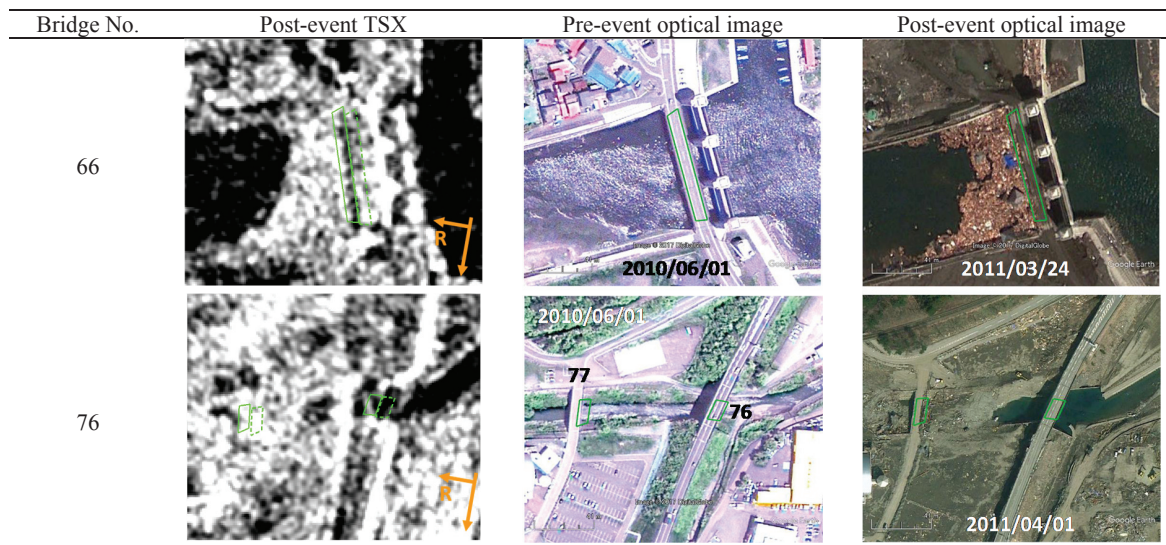
Fig. 7. Enlarged images for the two survived bridges that were classified as washed-away by visual interpretation.

backscatter coefficients within the shifted bridge polygons and the standard deviations (STD) are shown by the scatter plot in **Fig. 8**. Ten washed-away bridges are shown using red circles and the survived bridges are shown using green diamonds.

When a bridge was washed-away, the reflection from the deck disappeared, showing a low backscatter. Compared with the survived bridges, the average values of the washed-away bridges are smaller as shown in **Fig. 8**. Thus, a threshold value was applied on the average value of the backscattering coefficient to detect collapsed bridges. The threshold value changed continuously from -20.0 dB to -10.0 dB, and the sums of the producer accuracies for the washed-away and survived bridges were calculated one by one. The sum achieved the maximum value when the threshold value was set to -14.5 dB. This threshold value is also plotted in **Fig. 8**. Only one washed-away bridge, No.68, was excluded by this threshold value, whereas 5 out of the 48 survived bridges were misclassified as collapsed. The error matrix is presented in **Ta-**

Fig. 8. Scatter plot of the average value and the standard deviation of the backscattering coefficients within the shifted bridge polygons.

Table 3. Error matrixes using the thresholding of the backscattering coefficients within the shifted bridge polygons.

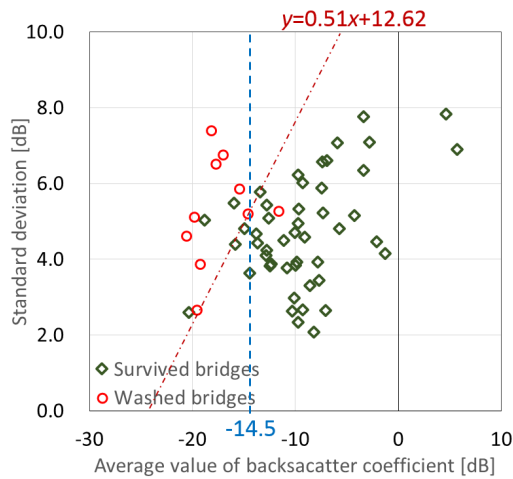|	(a) Average value			
$\mu < -14.5$ dB	Report of the NILIM			
	Washed-away	Survived	Total	User Acc.
TerraSAR-X Washed-away	9	5	14	64%
Survived	1	43	44	98%
Total	10	48	58	
Producer Acc.	90%	90%		**90%**

	(b) Combination of the average value and the standard deviation			
$0.51\mu - \sigma + 12.62$ > 0	Report of the NILIM			
	Washed-away	Survived	Total	User Acc.
TerraSAR-X Washed-away	9	3	12	75%
Survived	1	45	46	98%
Total	10	48	58	
Producer Acc.	90%	94%		**93%**

ble 3(a).

Because the threshold value was determined by the maximum sum of the producer accuracies, those for the washed-away bridges and for the survived ones were both 90%, very high values. However, the user accuracy for the washed-away bridges was 64%, a low value owing to the difference in the sample numbers. The number of the survived bridges was more than 5 times that of the washed-away bridges. The user accuracy for the survived bridges was 98%, a very high value. The overall accuracy was 90% and the Kappa coefficient was 0.68, showing good level of agreement.

For bridge No. 68, the strong reflection from the accumulated debris in the river resulted in a high average value of -11.60 dB. The 5 misclassified survived bridges showed low backscattering coefficients mainly due to two reasons. One reason is the existence of objects in front of the target, e.g., bridge No.1011 as shown in **Fig. 5**. The

other reason is the wrong location of the bridge polygons. Since the polygons were moved uniformly to the sensor direction, the layovers of several bridges with lower or higher clearance heights were not included in the shifted polygons, e.g., bridge No.76 in **Fig. 7**.

The other threshold value using both the average value (μ) and the STD (σ) value was also applied to detect the collapsed bridges. The washed-away bridges with higher backscattering values showed larger STD values due to strong reflection from the left piers or decks as in bridge Nos. 85 and 103. Thus, a combination of the average value and the STD value was used to classify the targets, as indicated by the red dashed line in **Fig. 8**. The combined factor value z is obtained by Eq. (1), which separates the washed-away and survived classes with the lowest omission errors. When z is larger than 0, the bridge was classified as washed-away.

$$z = 0.51\mu - \sigma + 12.62 \quad \ldots \ldots \ldots \ldots (1)$$

Using the combined factor z, only one washed-away bridge No. 85 was excluded, whereas 3 out of 48 survived bridges were misclassified as collapsed. The error matrix is presented in **Table 3(b)**. The producer accuracies for the washed-away bridges was 90%, and that for the survived bridges was 94%. The user accuracy for the washed-away bridges increased to 75%. The overall accuracy was 93% and the Kappa coefficient also increased to 0.77.

Thresholding using the statistics of the backscattering intensity showed promising results for the collapsed bridge extraction using only a post-event TSX image. However, it is difficult to use when the known training samples are few. The obtained threshold values are only effective for the SAR images under the same acquisition condition. Thus, another threshold value using the percentage of non-water regions was also attempted in this study.

Owing to the specular reflection of water surfaces, SAR images are useful for water extraction [10, 32]. Water regions in the post-event TSX image was extracted by a threshold value on the backscattering intensity. The threshold value was set according to the histogram of a coastal area including both water and urban regions, as shown in **Fig. 9**. The least point on the histogram between two peaks of the water and non-water regions was adopted, which was -12.3 dB. Then, the TSX intensity images was transformed to a binary image, where the water region is 0 and the non-water region is 1. Two examples around the washed-away bridge No.45 and the survived bridge No. 76 are shown in **Fig. 10**. The percentages (p) of the non-water region within the bridge polygons were calculated to classify the washed-away bridges. Considering the wrong locations of the polygons and parts with low backscatter in the layovers, bridges with a percentage less than 1/3 (33%) of the polygon were classified as washed-away. The error matrix is presented in **Table 4**.

One washed-away bridge No.68 was omitted whereas 4 survived bridges were misclassified as washed-way. In **Fig. 10**, bridge Nos.43 and 76 were the misclassified sur-
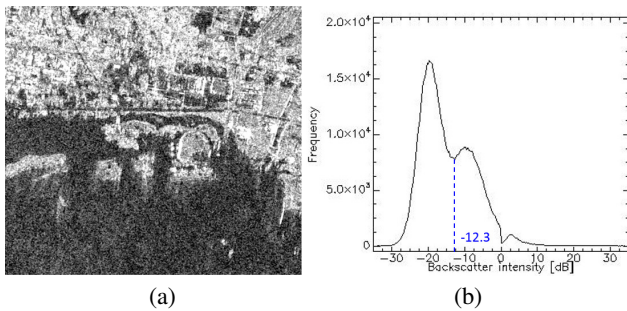
(a)   (b)

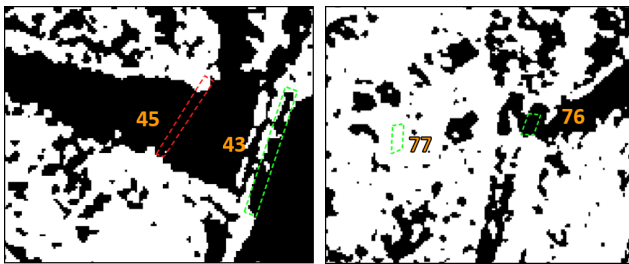**Fig. 9.** Costal area including both water and urban regions (a) and its histogram (b).

Fig. 10. Two examples of thresholding using a binary image, where the black region is water and the white region is not water.

Table 4. Error matrixes using thresholding of the percentage of water and non-water regions.

| $p < 33.3\%$ | Report of the NILIM | | | |
	Washed-away	Survived	Total	User Acc.
TerraSAR-X Washed-away	9	4	13	69%
Survived	1	44	45	98%
Total	10	48	58	
Producer Acc.	90%	92%		**91%**

vived bridges. The clearance height of bridge No. 43 was 3.5 m, lower than 6 m. The moved polygon covered only a part of the layover, which resulted in a low percentage. On the contrary, bridge No. 76 was higher than 6 m. The producer accuracy of the washed-away bridges was 90% whereas that of the survived bridges was 92%. The user accuracy of the washed-away bridges was 69%. The overall accuracy was 91% and the Kappa coefficient was 0.73, showing good level of agreement.

The accuracy of the thresholding percentage on the water-area was higher than that of using only the average value, but lower than that of using a combination of the average value and the STD. However, it can be easily applied to other SAR images, even without training samples.

6. Conclusions

In this study, the detection of the collapsed or washed-away bridges due to the 2011 Tohoku-oki, Japan earthquake and tsunamis was implemented using only post-event SAR intensity images and GIS data. First, the shapes of 58 bridges in the study area were created using the GIS dataset from roads and water. According to the clearance heights of 40 bridges reported by the NILIM, the created bridges polygons were shifted to the sensor direction uniformly considering a 6-m height to cover strong reflection zones.

Then, visual and automated interpretations were carried out to detect the washed-away/collapsed bridges. Compared with the NILIM report, the visual interpretation showed very high accuracy; however, it is time consum-

ing. The thresholding method using three factors were applied to the SAR image. The thresholding value on the combined factor of the average value and the standard deviation within the shifted bridge polygon showed the best result, where one washed-away bridge was omitted, and 3 survived bridges were misclassified. The overall accuracy was 93% and the Kappa coefficient was 0.78. However, the threshold values were affected by many elements, such as the condition of the bridges, the surrounding environment, and the acquisition condition of SAR images. Thus, the threshold value on the average values and the combined factors obtained in this study are difficult to use in other SAR images. In addition, the thresholding methods using both the average value and the combined factor require investigated bridges as training samples.

On the other hand, the thresholding method using the percentage of non-water region can be applied to other SAR images. The binary image can be easily created using the histogram of the backscattering coefficient. Although more experiments should be conducted in the future, the threshold value of 33% for the non-water region is considered as a common value for collapsed bridge detection. The overall accuracy of this method was 91% and the Kappa coefficient was 0.73.

One major reason for misclassification was the wrong locations of bridge polygons. As reported in previous studies [10, 12], crustal movements of more than 3 m occurred in the coastal area. Crustal movement and the uniform shift of the bridge polygons could cause mismatching between the bridge polygons and the TSX images. In our future work, a bridge height searching approach will be considered to improve the fit of the layover regions in a SAR image. In addition, the proposed method will be applied to other affected areas, such as Miyagi Prefecture.

References:
[1] National Institute for Land and Infrastructure Management (NILIM), "Annual report of road–related research in FY 2013," Technical Note of NILIM, No.843, 2013,

http://www.nilim.go.jp/lab/bcg/siryou/tnn/tnn0843.htm [in Japanese, available on Jan. 29, 2018]

[2] G. Shoji and T. Nakamura, "Damage assessment of road bridges subjected to the 2011 Tohoku Pacific earthquake tsunami," Journal of Disaster Research, Vol.12, No.1, pp. 79-89, doi: 10.20965/jdr.2017.p0079, 2017.

[3] K. Saito, R. J. S. Spence, C. Going, and M. Markus, "Using High-Resolution Satellite Images for Post-Earthquake Building Damage Assessment: A Study Following the 26 January 2001 Gujarat Earthquake," Earthquake Spectra, Vol.20, No.1, pp. 145-169, 2004.

[4] F. Yamazaki, Y. Yano, and M. Matsuoka, "Visual Damage Interpretation of Buildings in Bam City Using QuickBird Images Following the 2003 Bam, Iran, Earthquake," Earthquake Spectra, Vol.21, No.S1, pp. 329-336, doi: 10.1193/1.1650865, 2005.

[5] X. Tong, Z. Hong, S. Liu, X. Zhang, H. Xie, Z. Liu, S. Yang, W. Wange, and F. Bao, "Building-damage detection using pre- and post-seismic high-resolution satellite stereo imagery: A case study of the May 2008 Wenchuan earthquake," ISPRS Journal of Photogrammetry and Remote Sensing, Vol.68, pp. 13-27, doi: 10.1016/j.isprsjprs.2011.12.004, 2012.

[6] L. Dong and J. Shan, "A comprehensive review of earthquake–induced building damage detection with remote sensing techniques," ISPRS Journal of Photogrammetry and Remote Sensing, Vol.84, pp. 85-99, doi: 10.1016/j.isprsjprs.2013.06.011, 2013.

[7] P. T. B. Brett and R. Guida, "Earthquake damage detection in urban areas using curvilinear features," IEEE Transactions on Geoscience and Remote Sensing, Vol.51, No.9, pp. 4877-4884, doi: 10.1016/j.isprsjprs.2013.06.011, 2013.

[8] S. Plank, "Rapid damage assessment by means of multi-temporal SAR−A comprehensive review and outlook to Sentinel-1," Remote Sensing, Vol.6, pp. 4870-4906, doi:10.3390/rs6064870, 2014.

[9] D. Brunner, G. Lemoine, and L. Bruzzone, "Earthquake damage assessment of buildings using VHR optical and SAR imagery," IEEE Transactions on Geoscience and Remote Sensing, Vol.48, No.5, pp. 2403-2420, doi: 10.1109/TGRS.2009.2038274, 2010.

[10] W. Liu, F. Yamazaki, H. Gokon, and S. Koshimura, "Extraction of Tsunami Flooded Areas and Damaged Buildings in the 2011 Tohoku-oki, Japan Earthquake from TerraSAR-X Intensity Images," Earthquake Spectra, Vol.29, No.S1, pp. S183-2000, doi: 10.1193/1.4000120, 2013.

[11] H. Miura, S. Midorikawa, and M. Matsuoka, "Building damage assessment using high-resolution satellite SAR images of the 2010 Haiti earthquake," EERI Earthquake Spectra, Vol.32, No.1, pp. 591-610, doi: 10.1193/033014EQS042M, 2016.

[12] M. Wieland, W. Liu, and F. Yamazaki, "Learning change from Synthetic Aperture Radar images: Performance evaluation of a Support Vector Machine to detect earthquake and tsunami–induced changes," Remote Sensing, Vol.8, issue 10, No.792, doi: 10.3390/rs8100792, 2016.

[13] W. Liu, F. Yamazaki, B. Adriao, E. Mas, and S. Koshimura, "Development of building height data in Peru from high-resolution SAR imagery," Journal of Disaster Research, Vol.9, No.6, pp. 1042-1049, doi: 10.20965/jdr.2014.p1042, 2014.

[14] W. Liu, F. Yamazaki, and T. Sasagawa, "Monitoring of the recovery process of the Fukushima Daiichi nuclear power plant from VHR SAR images," Journal of Disaster Research, Vol.11, No.2, pp. 236-245, doi: 10.20965/jdr.2016.p0236, 2016.

[15] Y. Wang and Q. Zheng, "Recognition of roads and bridges in SAR images," Pattern Recognition, Vol.31, No.7, pp. 953-962, doi: 10.1016/S0031-3203(97)00098-8, 1998.

[16] U. Soergel, E. Cadario, A. Thiele, and U. Thoennessen, "Extraction of bridges over water in multi-aspect high-resolution InSAR data, International Archives of the Photogrammetry," Proceedings of Symposium of ISPRS Commission III Photogrammetric Computer Vision PCV'06, Vol.XXXVI, part 3, 2006.

[17] J. Luo, D. Ming, W. Liu, Z. Shen, M. Wang, and H. Sheng, "Extraction of bridges over water from IKONOS panchromatic data," International Journal of Remote Sensing, Vol.28, issue 16, pp. 3633-3648, doi: 10.1080/01431160601024226, 2007.

[18] U. Soergel, U. H. Gross, A. Thiele, and U. Thoennessen, "Feature extraction and visualization of bridges over water from high-resolution InSAR data and one orthophoto," IEEE Journal of Selected Topics in Applied Earth Observations and Remote Sensing, Vol.1, No.2, pp. 147-153, doi: 10.1109/JSTARS.2008.2001156, 2008.

[19] D. Chaudhuri and A. Samal, "An automatic bridge detection technique for multispectral images," IEEE Transactions on Geoscience and Remote Sensing, Vol.46, issue 9, pp. 2720-2727, doi: 10.1109/TGRS.2008.923631, 2008.

[20] M. Akiyama, D. M. Frangopol, M. Arai, and S. Koshimura, "Reliability of bridges under tsunami hazards: Emphasis on the 2011 Tohoku-oki earthquake," Earthquake Spectra, Vol.29, No.S1. pp. S295-S314, doi: 10.1193/1.4000112, 2013.

[21] G. Shoji and T. Nakamura, "Damage assessment of road bridges subjected to the 2011 Tohoku Pacific earthquake tsunami," Journal of Disaster Research, Vol.12, No.1, pp. 79-89, doi: 10.20965/jdr.2017.p0079, 2017.

[22] K. Inoue, W. Liu, and F. Yamazaki, "Detection of bridge damages due to Tsunami using multi-tempoeral high-resolution SAR images," Journal of Japan Association for Earthquake Engineering, Vol.17, issue 5, pp. 48-59, doi: 10.5610/jaee.17.5_48, 2017 (in Japanese).

[23] K. Jiang, C. Wang, H. Zhang, W. Chen, B. Zhang, Y. Tang, and F. Wu, "Damage analysis of 2008 Wenchuan earthquake using SAR images," Proceeding of 2009 IEEE International Geoscience and Remote Sensing Symposium, pp. V-108-V-111, doi: 10.1109/IGARSS.2009.5417722, 2009.

[24] T. Balz, D. Perissin, U. Soergel, and M. S. Liao, "Post–seismic infrastructure damage assessment using high-resolution SAR satellite data," Proceedings of 2nd International Conference on Earth Observation for Global Change, 12pp., 2009.

[25] T. Haraguchi and A. Iwamatsu, Detail map for the 2011 Tohoku-Oki earthquake and tsunamis, 2013 (in Japanese).

[26] AIRBUS DFENCE & SPACE, Radiometric calibration of TerraSAR-X Data, https://spacedata.copernicus.eu/documents/12833/14537/TerraSAR-X_RadiometricCalculations [available on Jan. 28, 2018]

[27] A. Lopes, R. Touzi, and E. Nezry, "Adaptive Speckle Filters and Scene Heterogeneity," IEEE Transactions on Geoscience and Remote Sensing, Vol.28, No.6, pp. 992-1000, doi: 10.1109/36.62623, 1990.

[28] Geospatial Information Authority of Japan (GSI), Fundamental Geospatial Data, http://www.gsi.go.jp/kiban/ [available on Jan. 28, 2018]

[29] W. Liu, K. Sawa, and F. Yamazaki, "Backscattering characteristics of bridges from high-resolution X-band SAR imagery," Proceedings of International Symposium on Remote Sensing 2017, pp. 324-327, 2017.

[30] H. Hirano, F. Yamazaki, and W. Liu, "Backscattering characteristics of bridges from airborne full-polarimetrics SAR images," Proceedings of the 38th Asia Conference on Remote Sensing, 9pp., 2017.

[31] P. Nakmuenwai, F. Yamazaki, and W. Liu, "Automated extraction of inundation areas from multi-temporal dual-polarization RADARSAT-2 images of the 2011 Central Thailand Flood," Remote Sensing, Vol.9, issue 1, No.78, doi:10.3390/rs9010078, 2017.

Name:
Wen Liu

Affiliation:
Assistant Professor, Graduate School of Engineering, Chiba University

Address:
1-33 Yayoi-cho, Inage-ku, Chiba 263-8522, Japan
Brief Career:
2010-2013 Ph.D. of Engineering, Chiba University
2013-2014 JSPS Postdoctoral Fellowship for Foreign Researchers, Tokyo Institute of Technology
2014- Assistant Professor, Graduate School of Engineering, Chiba University
Selected Publications:
● "Estimation of three-dimensional crustal movements in the 2011 Tohoku-oki, Japan earthquake from TerraSAR-X intensity images,"
Natural Hazards and Earth System Sciences, Vol.15, pp. 637-645, 2015c.
● "Extraction of Tsunami Flooded Areas and Damaged Buildings in the 2011 Tohoku, Japan Earthquake from TerraSAR-X Intensity Images,"
Earthquake Spectra, ERRI, Vol.29, No.S1, pp. S183-2000, 2013.
Academic Societies & Scientific Organizations:
● Japan Society of Civil Engineers (JSCE)
● Remote Sensing Society of Japan (RSSJ)
● Institute of Electrical and Electronics Engineers (IEEE)

Name:
Fumio Yamazaki

Affiliation:
Professor, Department of Urban Environment Systems, Chiba University

Address:
1-33 Yayoi-cho, Inage-ku, Chiba 263-8522, Japan
Brief Career:
1978 Research Engineer, Shimizu Corporation, Japan
1989 Associate Professor, Institute of Industrial Science, University of Tokyo
2001 Professor, Asian Institute of Technology (AIT), Bangkok, Thailand
2003 Professor, Department of Urban Environment Systems, Chiba University
Selected Publications:
● W. Liu and F. Yamazaki, "Detection of Crustal Movement from TerraSAR-X intensity images for the 2011 Tohoku, Japan Earthquake," Geoscience and Remote Sensing Letters, Vol.10, No.1, pp. 199-203, 2013.
● A. Meslem, F. Yamazaki, and Y. Maruyama, "Accurate evaluation of building damage in the 2003 Boumerdes, Algeria earthquake from QuickBird satellite images," Journal of Earthquake and Tsunami, Vol.5, No.1, pp. 1-18, 2011.
Academic Societies & Scientific Organizations:
● Japan Society of Civil Engineers (JSCE)
● American Society of Civil Engineering (ASCE)
● Seismological Society of America (SSA)
● Earthquake Engineering Research Institute, USA (EERI)